Available online at www.sciencedirect.com

SciVerse ScienceDirect

Ceramics International 39 (2013) 7669–7675

CERAMICS INTERNATIONAL

www.elsevier.com/locate/ceramint

Effect of donor dopants cerium and tungsten on the dielectric and electrical properties of high Curie point ferroelectric strontium niobate

Huanpo Ning[a,b,*], Haixue Yan[a,b], Zhipeng Gao[a], Xiaoyong Wei[a], Michael J. Reece[a,b]

[a]School of Engineering and Material Science, Queen Mary University of London, London, E1 4NS, UK
[b]Nanoforce Technology Ltd, London, E1 4NS, UK

Received 27 February 2013; received in revised form 5 March 2013; accepted 6 March 2013
Available online 13 March 2013

Abstract

The perovskite-like layered structure (*PLS*) $A_2B_2O_7$ compound $Sr_2Nb_2O_7$ was doped with donor dopants CeO_2 and WO_3 to explore their doping effect on its *A* and *B* site, respectively. The doped ceramics were prepared by Spark Plasma Sintering. For Ce doping on the *A* site, single phase was maintained up to 5 mol% Ce ($x=0.05$ in $(Sr_{1-x}Ce_x)_2Nb_2O_7$). For W doping on the *B* site, single phase was maintained at 2.5 mol% W ($x=0.025$ in $Sr_2(W_xNb_{1-x})_2O_7$). The cerium and tungsten doping both inhibited grain growth and changed the grain morphology, leading to less anisotropic grains. The Curie point T_c was obtained by measuring the temperature dependence of the dielectric constant and it was found to reduce for both Ce and W doped SNO. The W doped ceramics showed a diffuse ferroelectric phase transition at the Curie point. The DC resistivity of tungsten and cerium doped SNO increased compared to undoped SNO at temperatures below 700 °C. These results showed that both Ce and W had a strong influence on the dielectric and electrical properties of the $Sr_2Nb_2O_7$ ceramics.

Keywords: Ferroelectric; Doping; $A_2B_2O_7$; Strontium niobate; High Curie point

1. Introduction

Ferroelectrics with super-high Curie points are desirable in a number of high temperature applications, such as force, pressure and vibration sensors in materials manufacturing, automotive, aerospace, and nuclear power industries. Strontium niobate ($Sr_2Nb_2O_7$), as well as $La_2Ti_2O_7$, $Nd_2Ti_2O_7$, and $Pr_2Ti_2O_7$, which belongs to the perovskite-like layered structure (*PLS*) family, has been reported to be ferroelectric with a super-high Curie point (1342 °C) [1–4]. $Sr_2Nb_2O_7$ has an orthorhombic symmetry with the space group $CmC2_1$ at room temperature [5]. Recently, the ferroelectric and piezoelectric properties of ceramic $Sr_2Nb_2O_7$ prepared by spark plasma sintering (SPS) were investigated and its Curie point was characterised as 1327 °C [6,7].

Many investigations have shown that the doping of ferroelectrics is an effective approach for improving their properties, by influencing the Curie point, coercive field, and electrical resistivity. There have been some efforts in the past to dope SNO with various types of oxides to explore their effects on the microstructure and dielectric properties. The doping effect of La_2O_3 on $Sr_2Nb_2O_7$ (SNO) was investigated by Brahmaroutu et al. and it was found that the dielectric constant and loss decreased with increasing La^{3+} content [8]. The anisotropic grain growth of SNO was suppressed by the presence of La_2O_3 second phase at the grain boundaries, which pinned the grain boundaries. In other research, textured La doped SNO ceramic showed anisotropic thermal diffusivity and conductivity in the direction parallel and perpendicular to the perovskite layers [9]. Seraji et al. doped SNO with different amounts of V_2O_5, which resulted in an increase in dielectric constant and decrease in tangent loss. The single phase perovskite structure was maintained up to 15 at% vanadium and the doped SNO showed higher densities and the average grain size increased with increasing vanadium content [10]. The increased dielectric

*Corresponding author at: School of Engineering and Materials Science, Queen Mary University of London, Mile End Road, London E1 4NS, UK. Tel.: +44 77 4632 8394; fax: +44 20 7882 3390.
E-mail address: h.ning@qmul.ac.uk.(H. Ning)

0272-8842/$ - see front matter © 2013 Elsevier Ltd and Techna Group S.r.l. All rights reserved.
http://dx.doi.org/10.1016/j.ceramint.2013.03.019

constant was attributed to the fact that accommodating a smaller ion in an almost unchanged crystal unit cell results in more rattling space within the oxygen octahedron and hence increased ionic polarisation [11]. Vanadium ions has a smaller ionic radius (54 pm with coordination number CN of 6) compared with that of Nb^{5+} (64 pm with CN of 6) [12]. Recently, Gao et al. investigated the substitution of Barium on textured SNO ceramics, the T_c decreased with increasing Ba substitution and the highest piezoelectric constant d_{33} were obtained from $Sr_{1.8}Ba_{0.2}Nb_2O_7$ [13].

Donor doping, which uses a dopant with a higher valence than it replaces, has been investigated in many other ferroelectric materials. Cerium doping was shown to improve ferroelectric properties and the fatigue resistance of PZT by impeding the motion of oxygen vacancies [14]. The effects of tungsten doping were investigated for the Aurivillius ferroelectrics $SrBi_2Nb_2O_9$ (SBN) and $SrBi_2Ta_2O_9$ (SBT) [11,15]. For SBN ceramics doped with WO_3 on the *B* site, single phase was maintained when the doping level was below 2.5 mol%. The Curie points decreased while the peak dielectric constants increased after doping. Similar to the structure of SNO, the niobium ion in SBN is also located in the centre of the oxygen octahedron. Tungsten ions (W^{6+}) has a higher valence and smaller ionic radius (60 pm with CN of 6) compared with that of Nb^{5+} (64 pm with CN of 6) [12].

In this work, $Sr_2Nb_2O_7$ was doped with donor dopants CeO_2 and WO_3 on its *A* and *B* site, respectively. The ceramics were prepared by Spark Plasma Sintering (SPS). The effect of donor doping on its electrical, piezoelectric, ferroelectrics was investigated.

2. Experimental procedures

2.1. Sample preparation

The compositions of undoped and doped SNO were obtained by the mixed oxide route. The starting materials were $SrCO_3$ (99% purity, Avocado research chemicals Ltd), Nb_2O_5 (99.9% purity, Alfa Aesar), WO_3 (99.9% purity, Fluka Analytical), CeO_2 (99.9% purity, Aldrich). For *A* site doped SNO, compositions of $(Sr_{1-x}Ce_x)_2Nb_2O_7$ with $x=0.025$ and 0.05 were prepared from $SrCO_3$, Nb_2O_5 and CeO_2 powder. For *B* site doped SNO, compositions of $Sr_2(W_xNb_{1-x})_2O_7$ were prepared from $SrCO_3$, Nb_2O_5, and WO_3 powders, with $x=0.025$ and 0.05.

The starting powders were weighed according to the stoichiometric formula of the desired composition of the ferroelectric ceramics. They were mixed in a cylindrical nylon pot and ground by a rolling ball mill for 10 h with ethanol as the milling medium. After ball milling, the slurry mixture was dried and then sieved to break the particle agglomerates. The mixture of powders was calcined in an alumina crucible heated in a chamber furnace at 1200 °C for 4 h. The powders were then remilled for 24 h to reduce the particle size and break the agglomerates.

The synthesised powders were sintered by Spark Plasma Sintering SPS (HPD 25/1 FCT, Germany). The calcined powders were pressed in a 20 mm diameter graphite die and sintered at 1350 °C or 1425 °C under 80 MPa for 3 min. A heating rate of 100 °C/min was used for all the samples. The sintered ceramic disks were then annealed at 100 °C below their sintering temperature for 15 hours to remove any carbon contamination and reduction produced during SPS. The bulk density was measured by the Archimedes method.

2.2. Sample characterisation

X-ray diffraction (XRD) patterns for the powders were obtained with an X-ray diffractometer (Siemens D5000) using Cu K_α radiation. The microstructures of the ceramic samples were observed using a scanning electron microscope (SEM) (FEI, Inspect F). The samples for SEM were polished then thermally etched at 100 °C below their sintering temperatures for 15 min to reveal their grain structures. Electrodes were fabricated with fired-on platinum paste (Gwent Electronic Materials Ltd., C2011004D5) for electrical properties measurements. The frequency dependence of the dielectric constants and loss tangents was measured using a Precision Impedance Analyser (Agilent, 4294A). The temperature dependence of the dielectric constants and loss tangents were measured using a Precision LCR Meter (Agilent, 4284A) connected to a high temperature tube furnace. Samples for piezoelectric measurements were poled in silicone oil at 200 °C under a DC electric field. The piezoelectric constant d_{33} was measured using a quasi-static d_{33} metre (CAS, ZJ-3B). The accuracy of the d_{33} metre for measuring small coefficients was checked using X-cut quartz ($d_{33}=2.3\pm0.1$) pC/N [16]. The DC resistivity ρ was measured as a function of temperature using an electrometer (KEITHLEY, Model 6517A) with contacts to the samples in a high temperature furnace. All the resistivity data was recorded at 10 V after a 15 min holding time at high temperatures.

3. Results and discussions

Fig. 1(a) and (b) shows the XRD spectra of undoped, CeO_2 doped and WO_3 doped SNO powder, respectively. The single phase is maintained in doped SNO with 2.5 and 5 mol% Ce on the *A* site. For WO_3 doped SNO powder, it can be seen that the single phase is maintained at 2.5 mol% W doping on the *B* site, but an unidentified second phase was found when the doping level increased to 5 mol%. This solubility limit is similar to the case of W doping in Aurivillus material $SrBi_2Nb_2O_7$ [11].

Fig. 2(a)–(f) shows the SEM images of polished and thermally etched surfaces of undoped SNO and CeO_2 and WO_3 doped SNO ceramics sintered at 1350 °C and 1425 °C, respectively. The undoped SNO (Fig. 2(a) and (b)) has plate-liked grains. The 2.5 mol% and 5 mol% Ce doped SNO sintered at 1350 °C (Fig. 2 (c) and (d)) have high densities ($>$ 98%). However, the Ce doped samples sintered at 1425 °C have low densities ($<90\%$) and some large pores are present at the grain boundaries (not shown here), which may be caused by over-sintering. The grains exhibit lower aspect ratio (length/thickness) compared with those of the undoped SNO. Fig. 2(e) and (f) shows the single phase 2.5 mol% W doped SNO samples (densities $>98\%$) sintered at 1350 °C and 1425 °C. These W doped samples also show less anisotropic grain growth compared to undoped SNO. This could be explained by the fact that after doping the dopant segregates to the grain boundaries and impedes the grain growth along the in-

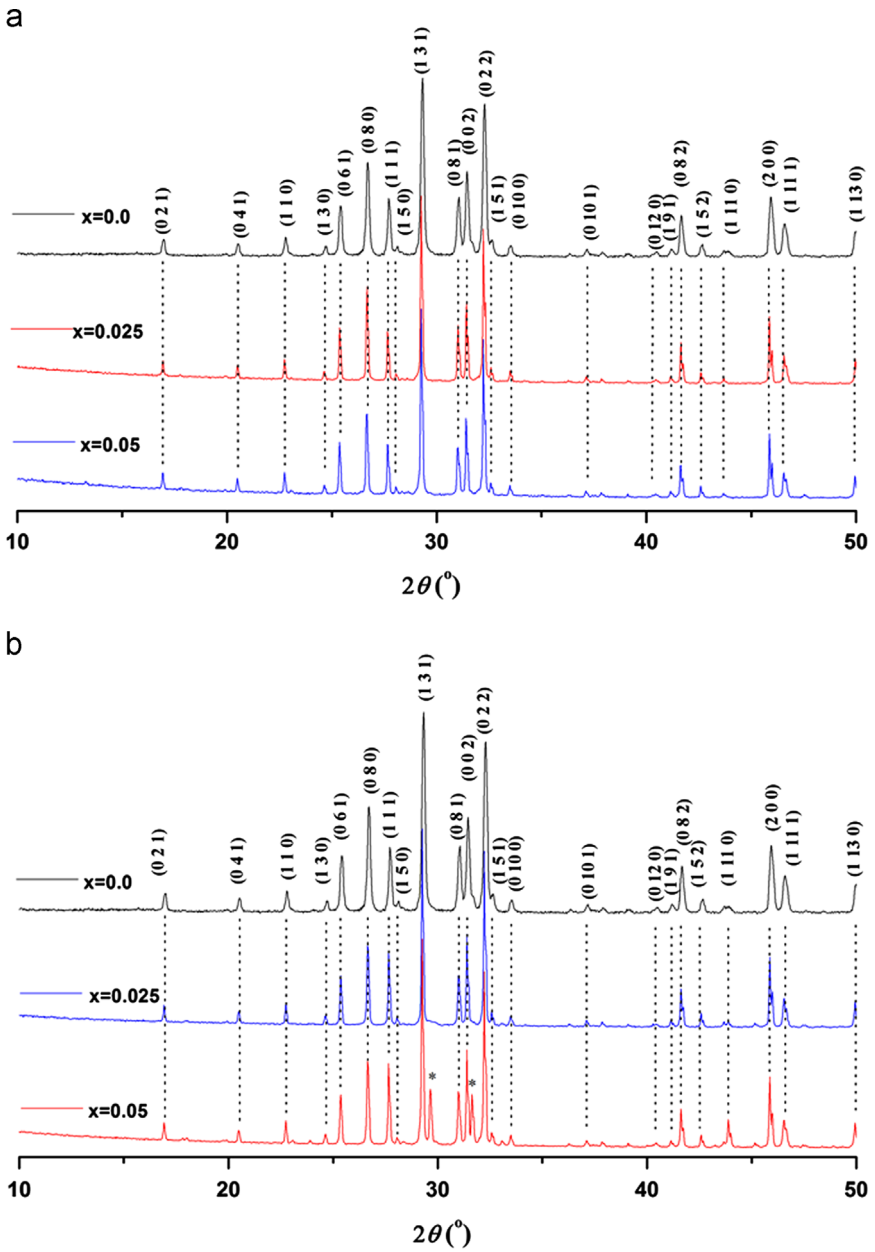

Fig. 1. (a) XRD patterns of $(Sr_{1-x}Ce_x)_2Nb_2O_7$ samples (x=0.0, 0.025, 0.05); (b) $Sr_2(W_xNb_{1-x})_2O_7$ samples (x=0.0, 0.025, 0.05). *highlights an unidentified second phase.

plane directions, so the grains become less anisotropic, as in the case of WO_3 doped $Bi_4Ti_3O_{12}$ [17].

The frequency dependence of dielectric constant ε_r and loss tangent D of CeO_2 and WO_3 doped SNO compared to undoped SNO at room temperature are shown in Fig. 3. The dielectric constants of all the samples are very stable within the measurement frequency range (100 Hz–10 MHz). It can be seen from Fig. 3(a) that the dielectric constant increased when increasing the CeO_2 doping level from 2.5 mol% to 5 mol%, compared to undoped SNO, while the loss tangent decreased in the lower frequency range (below 300 KHz). The 2.5 mol% W doped SNO samples showed similar behaviour to Ce doped samples (Fig. 3(b)). The increased dielectric constant could be due to the possible introduction of cation vacancies after donor doping to maintain charge neutrality [11]. These cation vacancies may increase the ionic polarisation and in turn contribute to the dielectric constant. Another explanation is that unchanged unit cells accommodating smaller ions with higher valence state would lead to an increased ionic polarisation [14]. The decreased loss tangent was attributed to the donor doping, which suppresses oxygen vacancies, as oxygen vacancies can act as space charge and contribute to the dielectric loss [15].

Fig. 4 shows the temperature dependence of real and imaginary part of the dielectric constant (ε_r and ε''), and loss tangent D of undoped and CeO_2 doped SNO at temperatures above 1000 °C and for frequencies of 100 KHz and 1 MHz frequency. The Curie point T_c is determined from the anomaly of the dielectric constant and it is 1302 ± 5 °C and 1285 ± 5 °C,

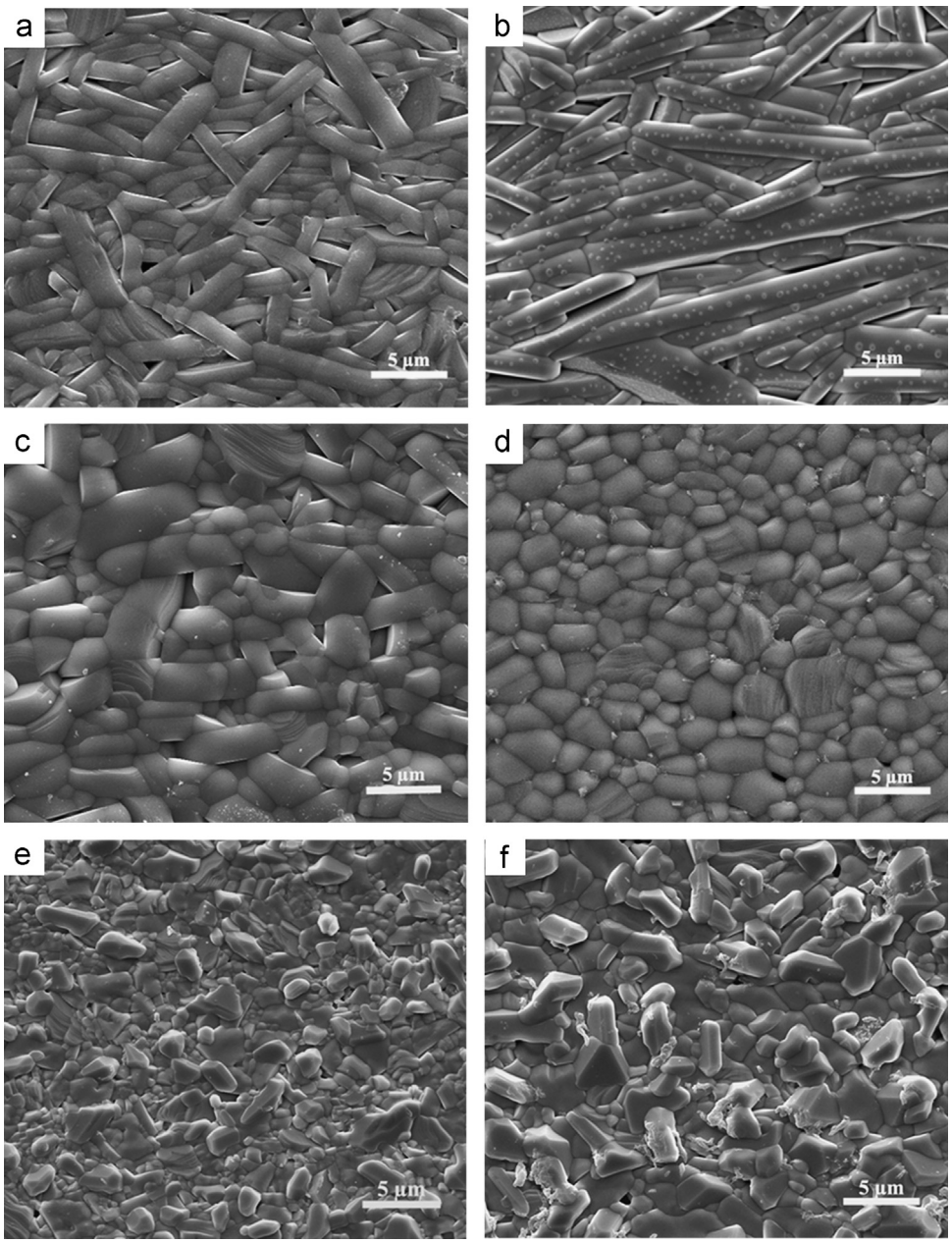

Fig. 2. SEM images of polished and then thermally etched surfaces of undoped and doped SNO sintered by SPS. The surfaces are viewed perpendicular to the SPS pressing direction. (a) undoped SNO sintered at 1350 °C; (b) undoped SNO sintered at 1425 °C; (c) 2.5 mol% Ce doped SNO ceramics sintered at 1350 °C; (d) 5 mol% Ce doped SNO sintered at 1350 °C; (e) 2.5 mol% W doped SNO samples sintered at 1350 °C; (f) 2.5 mol% W doped SNO samples sintered at 1425 °C.

for 2.5 mol% and 5 mol% Ce doped SNO, respectively. This is lower than that of undoped SNO (1327 ± 5 °C). The Curie peak maintains its position and sharpness after doping and also at different frequencies. There are also peaks corresponding to the Curie point in the temperature dependence of the dielectric loss ε'' curves at 1 MHz. However, these peaks were covered by the high conductivity at 100 KHz. The broad loss tangent peaks below the Curie point can be attributed to the domain wall movement and the minimum at the Curie point is due to the disappearance of the domain walls [18]. The decrease of Curie point can be attributed to the lower stability of ferroelectric structure of SNO after doping with ions with smaller radius and larger electronegativity; the cerium and tungsten ions have smaller ionic radius and larger electronegativity than Sr and Nb, respectively [12,19,20].

Fig. 5 shows the temperature dependence of real and imaginary part of the dielectric constant (ε_r and ε''), and loss tangent D of undoped and 2.5 mol% W doped SNO sintered at 1425 °C. The Curie point of tungsten doped SNO is 1308 ± 5 °C, which is also lower than that of undoped SNO. The WO_3 doped ceramic shows a diffuse ferroelectric phase transition at the Curie point, different from that for CeO_2 doped ceramic. As a result, there is no peak corresponding to the Curie point in the temperature dependence of the loss curves. The diffuse ferroelectric phase transition could be due to the convergence of a great number of local

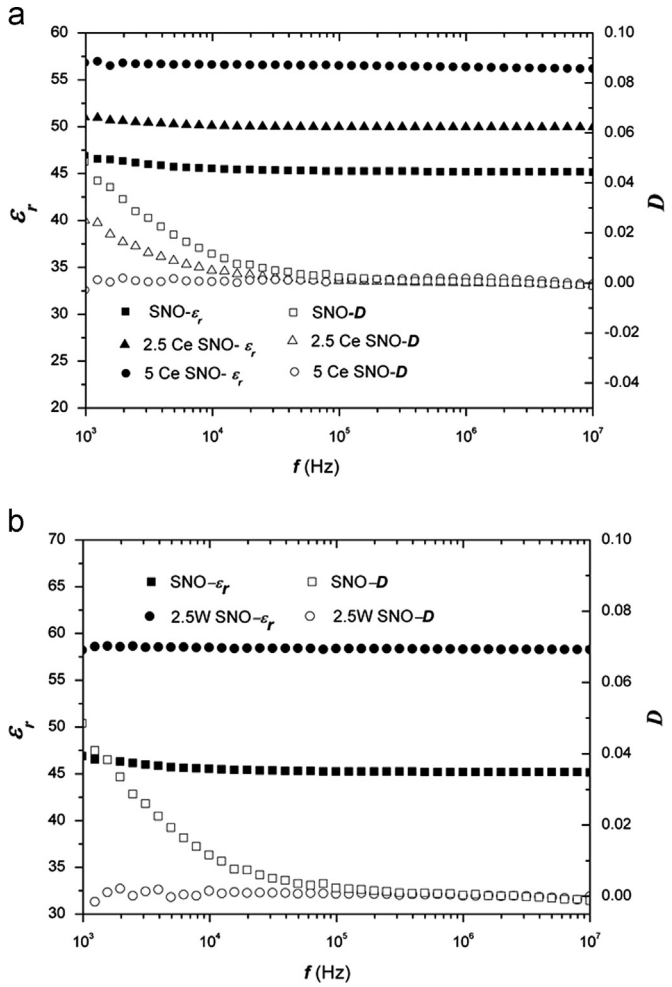

Fig. 3. Frequency dependence of dielectric constant ε_r and loss tangent D of: (a) 2.5 mol% and 5 mol% Ce doped SNO ceramics sintered at 1350 °C, compared to undoped SNO; (b) 2.5 mol% W doped SNO samples sintered at 1350 °C, compared to undoped SNO.

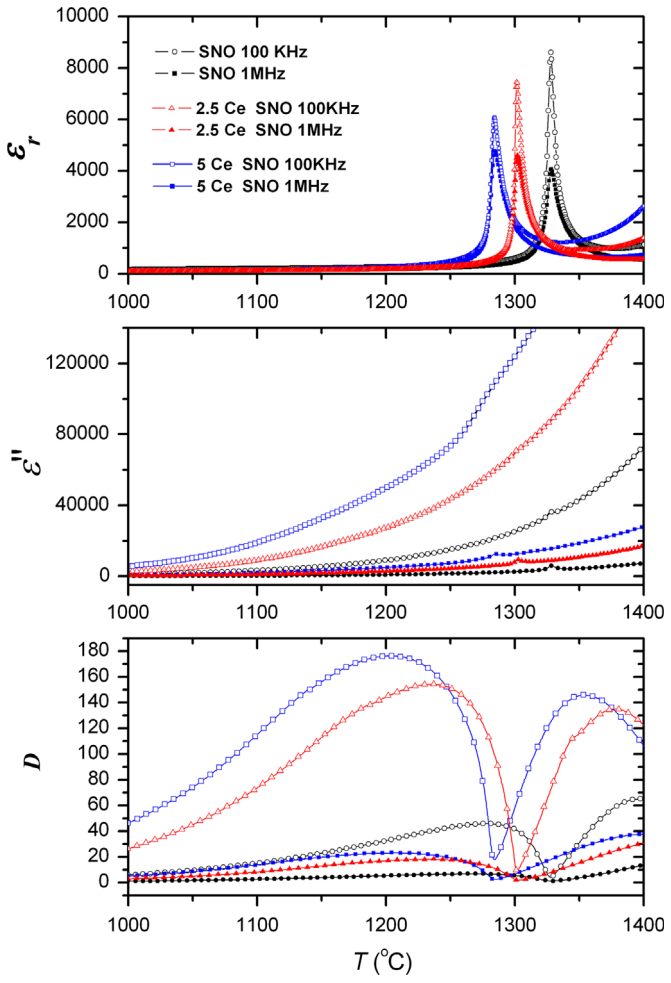

Fig. 4. Temperature dependence of dielectric constant ε_r, dielectric loss ε'' and loss tangent D of 2.5 mol% and 5 mol% Ce doped SNO and undoped SNO sintered at 1425 °C by SPS and measured at 1 MHz and 100 KHz.

ferroelectric phase transitions, which are caused by fluctuations in the local composition [21].

The undoped and Ce and W doped SNO samples sintered at 1350 °C were poled in silicone oil at 200 °C and 150 kV/cm for 5 min. The piezoelectric constant d_{33} of undoped, 0.25 and 0.5 mol% Ce doped SNO were 1.0, 1.2 and 1.5 pC/N, respectively. There was no detectable piezoelectric constant d_{33} value for the W doped SNO samples, which may be caused by an increase in the coercive field or reduced ferroelectric distortion after W doping. The differences of *A* site and *B* site doping may also indicate the ferroelectric behaviour mainly come from *B*–O coupling, similar with $BaTiO_3$ [22].

The DC resistivity of the undoped, 2.5 mol% W and 2.5 mol% Ce doped SNO ceramics as a function of temperatures is shown in Fig. 6(a). It can be observed that the resistivity of all the samples decreases with temperature. The resistivity of W and Ce doped SNO are both higher compared to undoped SNO at temperatures below 700 °C; while in the higher temperature region, the resistivity of doped SNO is slightly lower than undoped SNO, which is consistent with its higher dielectric loss at higher temperatures [18].

The experimental activation energy E_a was determined for the undoped, 2.5 mol% W and 2.5 mol% Ce doped SNO samples from the resistivity data in Fig. 6(b), according to the Arrhenius relationship [23]:

$$\rho = \rho_0 exp(E_a/kT)$$

where ρ is the resistivity, ρ_0 is a constant, E_a is the experimental activation energy, k is the Boltzmann constant and T is the absolute temperature. Taking natural logarithm of the Arrhenius equation yields:

$$ln\,\rho = E_a/kT + ln\rho_0$$

When lnρ is plotted against $1/T$ as shown in Fig. 6(b), it gives a straight line if the experimental activation energy E_a is constant, which can be determined from the slope of the line. For undoped SNO, the activation energy was derived as 0.88 eV. For both the 2.5 mol% W and Ce doped SNO samples, there is a slope change at about 500 °C, which indicates a change of activation energy at that temperature. The activation energy E_a in the low temperature regime (below 500 °C) is derived as 0.80 eV and 0.78 eV, respectively for 2.5 mol% W and Ce doped SNO samples. At the high temperature regime

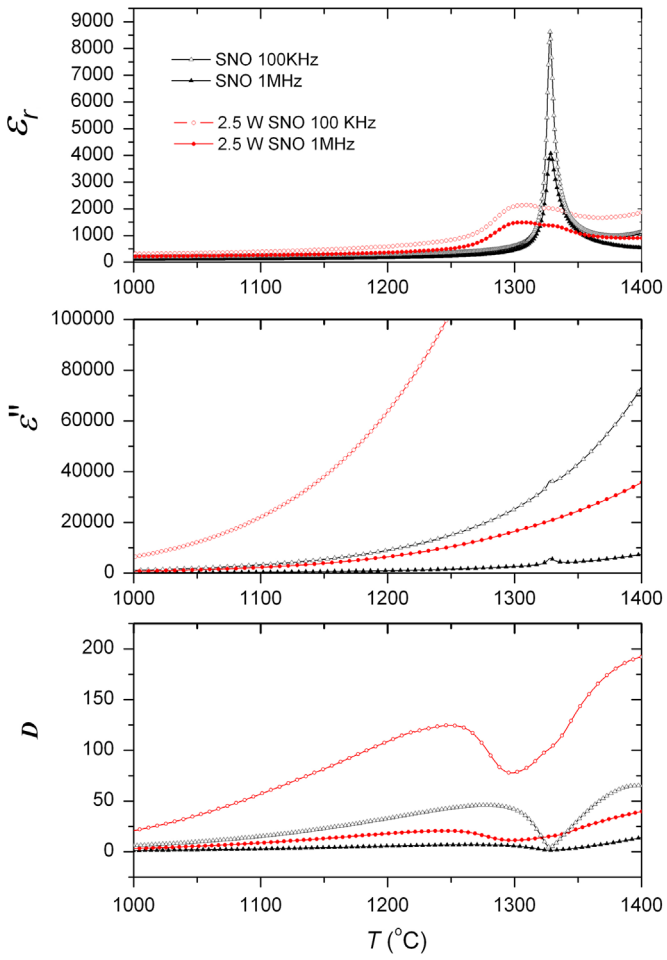

Fig. 5. Frequency dependence of dielectric constant, dielectric loss and loss tangent of 2.5 mol% W doped SNO sintered at 1425 °C and measured at 1 MHz and 100 KHz.

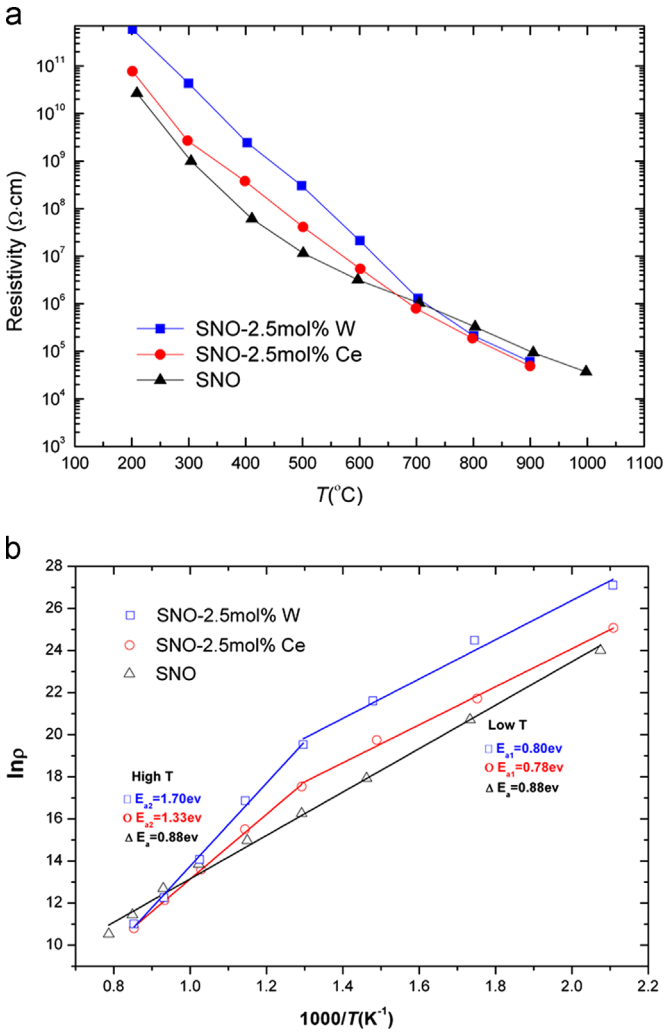

Fig. 6. (a) DC resistivity of SNO and SNO doped with 2.5 mol% W and 2.5 mol% Ce. (b) The corresponding activation energy E_a plot derived from (a).

(above 500 °C), E_a is calculated as 1.70 and 1.33 eV, respectively. The activation energy for undoped SNO and for doped SNO in the low temperature regime is close to that found for oxygen vacancies migration in perovskite oxides (0.9 eV) [24], which may indicate the main conductivity contribution is from oxygen vacancies. The larger E_a in the high temperature regime for doped SNO may reflect domination of the intrinsic electronic conductivity, which is about half of the band gap (2.88 eV) reported by Jeong et al. for donor doped SNO [25]. Therefore, the donor doping into SNO has compensated the oxygen vacancies and reduced the conductivities. While at very high temperatures (above 700 °C), the intrinsic electronic conductivity dominates, and the extrinsic charge carriers are exhausted, so that the different materials behave similarly.

4. Conclusions

$Sr_2Nb_2O_7$ was doped with donor dopants CeO_2 and WO_3 to explore the effect of doping on its properties.

Single phase is maintained up to 5 mol% cerium doping. Cerium doping on the *A* site inhibited anisotropic grain growth and led to grains with smaller aspect ratio. The Curie point decreased with increasing cerium doping level. Therefore, cerium doping can destabilise the ferroelectric phase, and cause a shift of the Curie point to lower temperature.

For tungsten doping on the *B* site, single phase is maintained up to 2.5 mol% doping level, but an unidentified second phase was found when the doping was increased to 5 mol%. Tungsten doping had a similar effect to cerium doping on the microstructure and the Curie point, except that the ferroelectric phase transition became diffuse. The samples could not be poled, which could be attributed to an increased coercive field or reduced ferroelectric distortion caused by the tungsten doping.

At room temperature, the dielectric constant increased with increasing cerium and tungsten doping, while the loss tangent decreased. The DC resistivity of doped SNO increased compared to undoped SNO at temperatures below 700 °C. This was attributed to the donor doping, which compensated the oxygen vacancies in SNO. The activation energy E_a in the lower temperature regime (below 500 °C) before and after doping is similar (about 0.8 eV), while the activation energy in the higher temperature regime (above 500 °C) increased after doping, especially for tungsten doping ($>$ 1.3 eV).

References

[1] S. Nanamatsu, M. Kimura, T. Kawamura, Crystallographic and dielectric properties of ferroelectric $A_2B_2O_7$ (a=Sr,B=Ta,Nb) crystals and their solid-solutions, Journal of the Physical Society of Japan 38 (1975) 817–824.

[2] S. Nanamatsu, M. Kimura, K. Doi, M. Takahashi, Ferroelectric properties of $Sr_2Nb_2O_7$ single crystal, Journal of the Physical Society of Japan 30 (1971) 300–301.

[3] H. Yan, H. Ning, Y. Kan, P. Wang, M.J. Reece, Piezoelectric ceramics with super-high Curie points, Journal of the American Ceramic Society 92 (2009) 2270–2275.

[4] Z. Gao, H. Yan, H. Ning, M.J. Reece, Ferroelectricity of $Pr_2Ti_2O_7$ ceramics with super-high Curie point, Advances in Applied Ceramics 112 (2013) 69–74.

[5] N. Ishizawa, F. Marumo, T. Kawamura, M. Kimura, Crystal-structure of $Sr_2Nb_2O_7$, a compound with perovskite-type slabs, Acta Crystallographica B 31 (1975) 1912–1915.

[6] H. Ning, H. Yan, M.J. Reece, Piezoelectric strontium niobate and calcium niobate ceramics with super-high Curie points, Journal of the American Ceramic Society 93 (2010) 1409–1413.

[7] H. Yan, H. Ning, H. Zhang, M.J. Reece, Textured high Curie point piezoelectric ceramics prepared by spark plasma sintering, Advances in Applied Ceramics 109 (2010) 139–142.

[8] B. Brahmaroutu, G.L. Messing, S. Trolier-McKinstry, Densification and anisotropic grain growth in $Sr_2Nb_2O_7$, Journal of Materials Science 35 (2000) 5673–5680.

[9] T.D. Sparks, P.A. Fuierer, D.R. Clarke, Anisotropic thermal diffusivity and conductivity of La-doped strontium niobate $Sr_2Nb_2O_7$, Journal of the American Ceramic Society 93 (2010) 1136–1141.

[10] S. Seraji, Y. Wu, S. Limmer, T. Chou, C. Nguyen, M. Forbess, G.Z. Cao, Processing and properties of vanadium doped strontium niobate, Materials Science and Engineering B-Advanced 88 (2002) 73–78.

[11] Y. Wu, S.J. Limmer, T.P. Chou, C. Nguyen, G.Z. Cao, Influence of tungsten doping on dielectric properties of strontium bismuth niobate ferroelectric ceramics, Journal of Materials Science Letters 21 (2002) 947–949.

[12] R.D. Shannon, Revised effective ionic-radii and systematic studies of interatomic distances in halides and chalcogenides, Acta Crystallographica A 32 (1976) 751–767.

[13] Z. Gao, H. Ning, C. Chen, R. Wilson, B. Shi, H. Ye, H. Yan, M.J. Reece, The effect of barium substitution on the ferroelectric properties of $Sr_2Nb_2O_7$ Ceramics, Journal of the American Ceramic Society, http://dx.doi.org/10.1111/jace.12121, in press.

[14] S.B. Majumder, Y.N. Mohapatra, D.C. Agrawal, Fatigue resistance in lead zirconate titanate thin ferroelectric films: effect of cerium doping and frequency dependence, Applied Physics Letters 70 (1997) 138–140.

[15] I. Coondoo, A.K. Jha, S.K. Agarwal, Enhancement of dielectric characteristics in donor doped Aurivillius $SrBi_2Ta_2O_9$ ferroelectric ceramics, Journal of the European Ceramic Society 27 (2007) 253–260.

[16] V.E. Bottom, Measurement of the piezoelectric coefficient of quartz using the fabry perot dilatometer, Journal of Applied Physics 41 (1970) 3941–3944.

[17] T. Jardiel, M.A. De La Rubia, M. Peiteado, Control of functional microstructure in WO_3-Doped $Bi_4Ti_3O_{12}$ ceramics, Journal of the American Ceramic Society 91 (2008) 1083–1087.

[18] K.H. Hardtl, Electrical and mechanical losses in ferroelectric ceramics, Ceramics International 8 (1982) 121–127.

[19] K. Chandramouli, G.S. Reddy, K. Ramam, Dielectric and piezoelectric properties of cerium-modified lead barium niobate ceramics, Journal of Alloys and Compounds 469 (2009) 609–616.

[20] J.G. Speight, Lange's Handbook of Chemistry, 16th ed., McGraw-Hill, New York, 2005.

[21] V.A. Isupov, Phenomena at transformation from sharp to diffuse ferroelectric phase transition, Ferroelectrics 143 (1993) 109–115.

[22] R.E. Cohen, Origin of ferroelectricity in perovskite oxides, Nature 358 (1992) 136–138.

[23] A.J. Moulson, J.M. Herbert, Electroceramics: Materials, Properties, Applications, 2nd ed., John Wiley & Sons Ltd, Chichester, 2003.

[24] L. Warren, K. Vanheusden, D. Dimos, G.E. Pike, B.A. Tuttle, Oxygen vacancy motion in perovskite oxides, Journal of the American Ceramic Society 79 (1996) 536–538.

[25] D.E. Jeong, G.M. Ha, S.M. Won, G.H. Kim, K.H. Pak, H.P. Borse, M.S. Ji, S.J. Lee, Photophysical properties and electronic structure of highly donor doped (110) layered perovskite material, Journal of the Korean Physical Society 49 (2006) 671–674.